

Exotic Attractors of the Nonequilibrium Rabi-Hubbard Model

M. Schiró,¹ C. Joshi,^{2,3} M. Bordyuh,⁴ R. Fazio,^{5,6} J. Keeling,³ and H. E. Türeci⁴

¹*Institut de Physique Théorique, Université Paris Saclay, CNRS, CEA, F-91191 Gif-sur-Yvette, France*

²*Department of Physics, University of York, Heslington, York YO10 5DD, United Kingdom*

³*SUPA, School of Physics and Astronomy, University of St. Andrews, St. Andrews KY16 9SS, United Kingdom*

⁴*Department of Electrical Engineering, Princeton University, Princeton, New Jersey 08544, USA*

⁵*ICTP, Strada Costiera 11, I-34151 Trieste, Italy*

⁶*NEST, Scuola Normale Superiore and Istituto Nanoscienze-CNR, I-56127 Pisa, Italy*

(Received 15 March 2015; revised manuscript received 14 February 2016; published 8 April 2016)

We explore the phase diagram of the dissipative Rabi-Hubbard model, as could be realized by a Raman-pumping scheme applied to a coupled cavity array. There exist various exotic attractors, including ferroelectric, antiferroelectric, and incommensurate fixed points, as well as regions of persistent oscillations. Many of these features can be understood analytically by truncating to the two lowest lying states of the Rabi model on each site. We also show that these features survive beyond mean field, using matrix product operator simulations.

DOI: 10.1103/PhysRevLett.116.143603

Introduction.—A number of recent experimental breakthroughs [1–4] have spurred the investigation of non-equilibrium properties of hybrid quantum many-body systems of interacting matter and light. Characterized by excitations with a finite lifetime, when sustained by finite-amplitude optical drives they display steady-state phases that are generally far richer [5–10] than their equilibrium counterparts [11,12]. Critical phenomena in these open driven-dissipative systems often come with genuinely new properties and novel dynamic universality classes, even when an effective temperature can be identified [13–17], a statement that can be made robust in renormalization group calculations [18,19]. Coupled cavity QED systems [20–22] have emerged as natural platforms to study many-body physics of open quantum systems. The current fabrication and control capabilities in solid-state quantum optics allows us to probe lattice systems [23–31] in the mesoscopic regime, providing a first glimpse into how macroscopic quantum behavior may arise far from equilibrium. It is therefore of interest to identify a physical system where a nonequilibrium phase transition (i) can be studied—at least in principle—in the thermodynamic limit, (ii) can be compared to an equilibrium analogue through a proper limiting procedure, and (iii) can be easily realized in an architecture that is currently available.

The Rabi-Hubbard (RH) model [32] represents the minimal description of coupled cavity QED systems, explicitly containing terms which do not conserve the particle number. These terms are relevant for the low-frequency behavior of the coupled system and their inclusion lead, in equilibrium, to a Z_2 -symmetry breaking phase transition between a quantum disordered paraelectric phase and an Ising ferroelectric [32,33]. The equilibrium RH transition requires a sizable intercavity hopping or light-matter interaction, of the order of the transition

frequency of cavities and qubits [32]. While such ultra-strong coupling regimes have recently been realized in specific circuit QED architectures [34], they are hard to achieve in lattice cavity QED settings. To overcome this challenge it is therefore crucial to engineer effective realizations of the RH model by, e.g., suitably designed driving schemes. In this Letter, we study the behavior of such a scheme that leads to a RH model with highly tunable parameters and in a fully nonequilibrium regime.

The interplay of drive and dissipation results in exotic attractors, remarkably different from thermal equilibrium, with rich patterns of symmetry breaking including incommensurate and antiferroelectric ordering. In the following, we identify and explain these orders, and the associated phase transitions using a variety of mean field approaches and then confirm the qualitative picture by simulating a one-dimensional open RH model with a matrix product operator (MPO) approach [35–39].

Tunable open Rabi-Hubbard model.—Recently, several proposals to engineer effective light-matter interactions by suitable designed driving schemes have appeared [40–43], based on a variety of platforms including superconducting circuit QED, impurities in diamond, and ultracold atoms [4]. Here for concreteness we consider a lattice of coupled cavity-QED systems, where on each lattice site n there is a four-level system which is driven and coupled to a cavity mode (see Fig. 1). We can write the full Hamiltonian as $\hat{H} = J \sum_{\langle nm \rangle} \hat{a}_n^\dagger \hat{a}_m + \sum_n \hat{h}_n^{4LS}$, where J is the hopping rate, \hat{a}_n^\dagger , \hat{a}_n are creation and annihilation operators of the cavity mode, while $\hat{h}_n^{4LS} = \omega_0 a_n^\dagger \hat{a}_n + \sum_{j=0,1,r,s} E_j |j\rangle_n \langle j|_n + \hat{H}_{\text{int}} + \hat{H}_{\text{drive}}(t)$ describes the driven four-level atom coupled to cavity. The key idea of this Raman pumping scheme [40] is that the cavity mediates transitions between states $0 \leftrightarrow r$, $1 \leftrightarrow s$ (blue arrows in Fig. 1), i.e., $\hat{H}_{\text{int}} = \hat{a}_n (g_r |r\rangle \langle 0| + g_s |s\rangle \langle 1|) + \text{H.c.}$

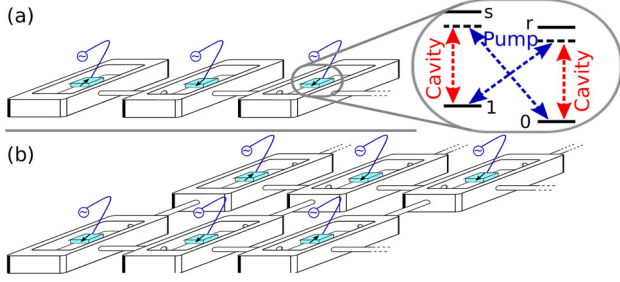


FIG. 1. Schematic array of coupled cavities in (a) 1D or (b) 2D, containing “Raman-driven” qubits. Inset: Cartoon of Raman driving: two low-lying levels of each artificial atom are connected via excited states. The strength of the drive determines the effective atom-cavity coupling [44].

while a two-frequency pump drives the transitions $1 \leftrightarrow r$, $0 \leftrightarrow s$ (red arrows in Fig. 1), i.e., $\hat{H}_{\text{drive}}(t) = \frac{\Omega_r}{2} e^{-i\omega_r t} |r\rangle\langle 1| + \frac{\Omega_s}{2} e^{-i\omega_s t} |s\rangle\langle 0| + \text{H.c.}$ The combined effect of light-matter interaction and drive is to induce an effective direct coupling between the two low-lying atomic states. More formally, this can be shown by the standard procedure of first eliminating the explicit time-dependence of $H_{\text{drive}}(t)$ moving to a rotating frame and then eliminating the excited states to obtain an effective model for the cavity photon and the states $|0\rangle$, $|1\rangle$ acting as an effective qubit [44]. The effective Hamiltonian takes the generalized RH form

$$\hat{H}_{\text{RH}} = -J \sum_{\langle nm \rangle} \hat{a}_n^\dagger \hat{a}_m + \sum_n \hat{h}_n, \quad (1)$$

$$\hat{h}_n = \frac{\omega_0}{2} \hat{\sigma}_n^z + \omega \hat{a}_n^\dagger \hat{a}_n + (g \hat{a}_n^\dagger \hat{\sigma}_n^- + g' \hat{a}_n^\dagger \hat{\sigma}_n^+ + \text{H.c.}), \quad (2)$$

where on each site n we have now a two-level system, $\hat{\sigma}^+ = |1\rangle\langle 0|$, $\hat{\sigma}^- = |0\rangle\langle 1|$. The corotating and counterrotating couplings g , g' , as well as the effective cavity and qubit frequencies ω , ω_0 are tunable through the amplitude and frequency of the Raman drive [44]. We stress that although described by a static Hamiltonian, the problem retains its nonequilibrium character since cavity and qubit excitations are coupled to baths which are described, in the rotating frame, by a nonthermal distribution of modes. To account for the dissipative nature of the problem, we use a master equation for the density matrix of the system $\dot{\rho} = -i[H_{\text{RH}}, \rho] + \sum_n \mathcal{D}_n[\rho]$, where the Liouvillian has the form

$$\mathcal{D}_n[\rho] = \gamma \mathcal{L}[\hat{\sigma}_n^-, \rho] + \kappa \mathcal{L}[\hat{a}_n, \rho], \quad (3)$$

with $\mathcal{L}[\hat{X}, \rho] = 2\hat{X}\rho\hat{X}^\dagger - \hat{X}^\dagger\hat{X}\rho - \rho\hat{X}^\dagger\hat{X}$ the Lindblad superoperator. Here, κ and γ are (constant) decay rates.

The RH Hamiltonian in Eq. (1), as well as the dissipator in Eq. (3), have a global Z_2 parity symmetry, corresponding to a simultaneous change of sign of cavity and qubit operators $(\hat{a}^\dagger, \hat{\sigma}^+) \rightarrow (-\hat{a}^\dagger, -\hat{\sigma}^+)$. As a result, on general

grounds we can expect a steady state phase diagram with a symmetric phase, where any quantity which is odd under parity will vanish, i.e., $\langle \hat{\sigma}_n^x \rangle = \langle \hat{a}_n + \hat{a}_n^\dagger \rangle = 0$, and a phase with broken Z_2 parity symmetry.

Mean Field Theory of open Rabi-Hubbard Model.—To characterize the steady state properties of open RH model we make a mean-field ansatz for the system density matrix $\rho = \otimes_n \rho_n$. The dynamics reduces to a collection of inequi-

valent single-site RH problems $\partial_t \rho_n = -i[\hat{h}_n, \rho_n] + \mathcal{D}_n[\rho_n] + iJ[\alpha_n^* \hat{a}_n + \alpha_n \hat{a}_n^\dagger, \rho_n]$ in a self-consistent field $\alpha_n = \sum_{m: \langle mn \rangle} \text{Tr}(\rho_m \hat{a}_m)$. Such an ansatz follows the standard concept of mean-field theory, that each site sees only the average field of its neighbors [45]. Thus, as for all mean-field theories, it becomes increasingly accurate in higher dimensions, as high coordination suppresses fluctuation contributions beyond the mean field.

We start our discussion from the $g = g'$ case. In order to identify the phase boundary and to guide our analysis of the ordered phase, it is useful to first study the instability of the homogeneous normal state, by adding a small perturbation to the factorized density matrix as done in Ref. ([46]), i.e., $\rho = \otimes_n (\rho_{ss} + \delta\rho_n)$ where ρ_{ss} is the normal state density matrix obtained from the equation $\mathcal{M}_n[\rho] \equiv -i[\hat{h}_n, \rho_{ss}] + \mathcal{D}_n[\rho_{ss}] = 0$. Considering the one-dimensional case for simplicity and taking the fluctuations as plane waves of the form $\delta\rho_n = \sum_k \delta\rho_k e^{i(kn - \nu_k t)} + \text{H.c.}$, we obtain the equation of motion

$$-i\nu_k \delta\rho_k = \mathcal{M}_n[\delta\rho_k] - t_k \{ \text{Tr}(\hat{a} \delta\rho_k) i[\hat{a}^\dagger, \rho_{ss}] + \text{H.c.} \}, \quad (4)$$

where $t_k = -2J \cos(k)$ is the one-dimensional bare photon dispersion. A positive imaginary part of the frequency, $\text{Im}[\nu_k] > 0$, signals the growth of fluctuations with momentum k and the onset of normal state instability. The results of linear stability analysis are plotted in Fig. 2(a) where we can see the phase boundary in the (g, J) plane and, in color scale, the wave vector of the most unstable mode. Two remarkable features immediately appear. First, the boundary has a “nose” at small J , i.e., a minimal critical J required to enter the ordered phase. This is in contrast to the ground state phase diagram [32], in which the critical value of J asymptotically approaches 0 as $g = g' \rightarrow \infty$. In addition, the nature of the broken symmetry phase itself shows an interesting evolution across the phase diagram. As the most unstable wave vector evolves smoothly from $k = 0$, characteristic of a uniform ferroelectric (F) phase, toward $k = \pi/2$, the wavelength must pass through irrational values, corresponding to an instability towards incommensurate order. Such symmetry-broken inhomogeneous states require us to model a finite length array and we consider in panels (b)–(d) a 16 site array with periodic boundary conditions. We focus on correlations $\langle \hat{\sigma}_n^x \hat{\sigma}_{n+l}^x \rangle$ which at short distance [$l = 1$, panels (b),(c)] are

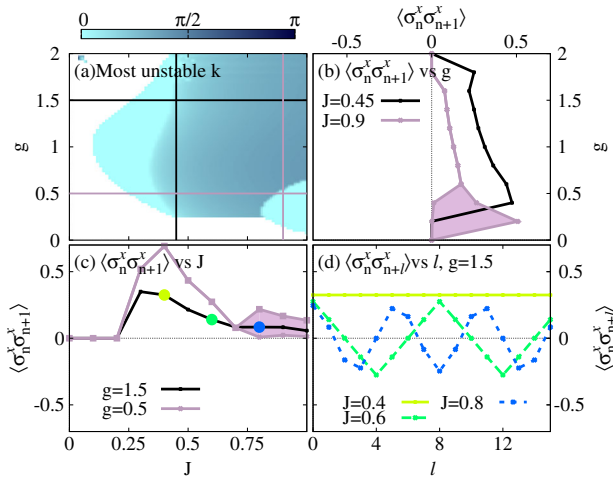


FIG. 2. (a) Mean-field phase diagram of driven-dissipative Rabi-Hubbard model at $g = g'$, $\omega = \omega_0$, calculated by linear stability analysis of the normal state. The color scale indicates the wave vector of the most unstable mode. This wave vector predicts the ordering seen by finding the steady state solution for a chain of 16 cavities, as shown in panels (b)–(d). Panels (b),(c) show the nearest-neighbor correlations on the vertical and horizontal cuts marked in panel (a). The shaded region shows the envelope of the limit cycle oscillations of the correlation function. Panel (d) shows the correlation vs separation at the three points marked in panel (c), revealing the incommensurate ordering. Parameters (also for the other figures): $\omega = \omega_0 = 1$, $\kappa = 0.1$, $\gamma = 0.05$.

ferroelectric but alternate in sign as a function of distance l [panel (d)] revealing the inhomogeneous ordering. The finite length of the array is enough to see the trend of density-wave period vs hopping J , although it prevents a continuous evolution of the period. Such an incommensurate order is absent in equilibrium, where the minimum free energy state always has a constant phase across the array. Another unique feature of the steady state phase diagram is the existence of limit cycles [47–50]. Within the linear stability analysis, a limit cycle can be anticipated if the normal state becomes unstable via a Hopf bifurcation [51]—i.e., if there are a pair of eigenvalues $\nu_k = \pm\nu'_k + i\nu''_k$ that simultaneously become unstable, leading to an oscillatory instability. This in fact occurs for the region around $g = 0.25$, $J > 0.8$ where the most unstable k returns to $k = 0$. The existence of the limit cycle is confirmed by direct time evolution of the equations of motion; in Figs. 2(b) and 2(c) the shaded region shows the envelope of the limit cycle oscillations of the correlation function.

As we move away from the pure RH limit and consider $g \neq g'$ two main features arise [44], namely (i) the shape of the phase boundary changes with multiple separate ordered regions and quite remarkably (ii) for certain values of light-matter couplings g' , g we find an instability at $k = \pi$ corresponding to antiferroelectric (AF) order, where qubit and photon polarization alternates in sign between even and odd sites of the array, i.e., $\langle \sigma_n^x \rangle, \langle a_n + a_n^\dagger \rangle \sim (-1)^n$. This is

a particularly striking result, considering that the effective qubit-qubit interaction in the equilibrium ground state would be ferromagnetic [32], and further pinpoints the profound differences between the open driven-dissipative, and equilibrium incarnations of the RH model.

Even extending the thermodynamics to a negative effective temperature, it is not possible to explain all the features identified, such as limit cycles or incommensurate order. Predicting the pattern of steady states clearly requires going beyond equilibrium thermodynamics.

Effective spin model.—We now introduce an effective spin 1/2 model which captures the essential physics of the RH model [44]. We start by considering the single site RH model; i.e., we set $J = 0$ in Eq. (1), and plot in figure Figs. 3(a)–3(d) the energies and the steady state populations of its eigenstates as a function of g , for two different values of g'/g . We first consider the $g' = g$ case, panels (a), (c). Here, we notice that (i) the two low-lying states become almost degenerate for large g and (ii) they are the only states effectively populated. The idea is then to truncate the local Hilbert space to the two lowest energy states of the on-site RH Hamiltonian that we denote $|\pm\rangle_n$ according to their (opposite) parity. Within this space the on-site Hamiltonian simply becomes $\hat{h}_n^{\text{eff}} = \Delta \hat{\tau}_n^z$, while the Liouvillian becomes $\mathcal{D}_n^{\text{eff}}[\rho] = \gamma \mathcal{L}[S_- \hat{\tau}_n^- + S_+ \hat{\tau}_n^+, \rho] + \kappa \mathcal{L}[A_- \hat{\tau}_n^- + A_+ \hat{\tau}_n^+, \rho]$, where $\hat{\tau}_n^{i=x,y,z}$ are Pauli operators, and $\Delta = E_- - E_+$ is the splitting between the lowest energy odd and even parity states, and A_\pm, S_\pm are the matrix elements $A_\pm = {}_n \langle \pm | \hat{a}_n | \mp \rangle_n, S_\pm = {}_n \langle \pm | \hat{\delta}_n^- | \mp \rangle_n$. Note that the values of Δ, A_\pm, S_\pm are all functions of g, g', ω, ω_0 , found by diagonalizing the Rabi model [32,44]. In addition, these local effective two-level systems are coupled by an anisotropic exchange mediated by photons $J_{x,y} \sim J(A_- \pm A_+)$, which gives rise to an effective Hamiltonian in the transverse field Ising universality class.

We now show that the effective model captures the salient features of the RH model. First, in the limit of large $g = g'$, one can show that there is an exponentially small splitting $\Delta = \omega_0 \exp(-2g^2/\omega^2)$ and the matrix elements become almost identical $A_\pm = (-1 \pm \Delta/\omega)g/\omega$. As a consequence, the hopping is predominantly an Ising coupling $\hat{\tau}_n^x \hat{\tau}_{n+1}^x$, and, in d dimensions, one can derive a simple expression for the critical hopping

$$J_{\text{crit}} \approx \frac{1}{d} \left[\frac{\kappa^2 g^2}{\omega^3} + \frac{\omega^3}{16g^2} \right]. \quad (5)$$

Such an expression clearly explains the appearance of a minimum $J_{\text{crit}} > \kappa/2d$ for any finite loss κ , as opposed to the exponentially small critical coupling $J_{\text{crit}}^{\text{eq}} \sim \Delta$ found in equilibrium. Furthermore, Eq. (3) matches the linear-stability phase boundary remarkably well, see Fig. 3(e). In addition, it shows that as the loss $\kappa \rightarrow 0$, the nose will move toward $g \rightarrow \infty, J \rightarrow 0$ consistent with the equilibrium phase diagram [32].

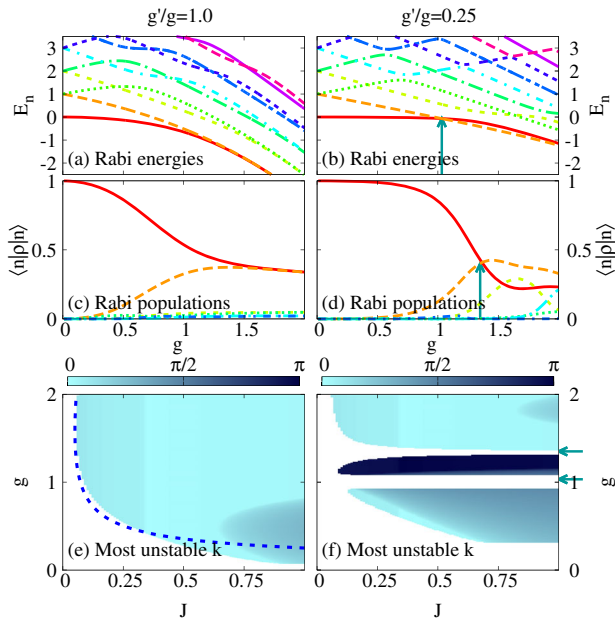


FIG. 3. Properties of the effective spin model $g'/g = 1$ (left) and $g'/g = 0.25$ (right). (a),(b) Eigenvalues and (c),(d) normal state populations of the eigenstates of the Rabi model. The effective spin 1/2 model truncates to only the first two levels: the solid (red) and long-dashed (orange) curves. For $g'/g = 0.25$, the energies and populations of these levels cross, as marked by an arrow. (e),(f) Phase diagram of the effective Ising model as obtained by linear stability analysis, with color scale indicating the wave vector of the most unstable mode, and by mean field analysis (dashed line). Arrows in panel (f) mark the crossing points marked in panels (b),(d).

We next consider the case $g' \neq g$, and plot in Figs. 3(b) and 3(d) the energy levels and steady state population of the single site RH model. In this case there are energy level crossings (see arrow), corresponding to a change in sign of local transverse field $\Delta = E_- - E_+$ for our effective spin model. This has interesting consequences for the lattice model as we see in panel (f), which shows the phase diagram as obtained from linear stability analysis for $g' = g/4$. At the degeneracy point the ordered phase is suppressed, and beyond the crossing point an AF instability occurs (see bottom arrow), as recently observed in the transverse field Ising model [52]. Upon further increasing the coupling g a further transition to a normal phase occurs, followed by a recovery of ferroelectric order (top arrow). This latter effect is associated with a population inversion between the $|\pm\rangle$ eigenstates, as one can see in the level occupations shown in Fig. 3(d).

Thus, the sequence of F-AF-F can be explained as follows: At small g the ground state is that of even parity, and this state is the most occupied, leading to F. On increasing g , first the energy ordering of the odd and even parity states is swapped, leading to AF, where the even parity state is most occupied despite being of higher energy. Then, the occupation of the even and odd parity states inverts, so that once again the

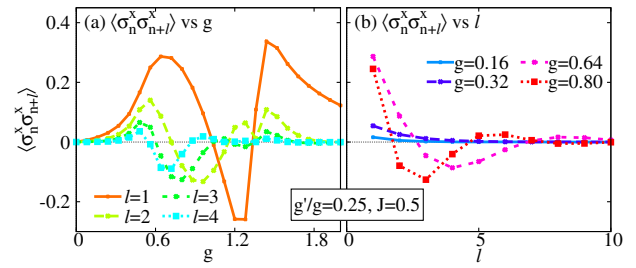


FIG. 4. Correlations of the one-dimensional effective spin 1/2 model, evaluated in an infinite-MPO approach for $g'/g = 0.25$, $J = 0.5$. (a) Correlations vs g , at various separations l between sites. (b) Correlations vs separation l at various values of g . These confirm the ordering seen in mean-field theory, specifically the sequence of F-AF-F on increasing g , but show only short-range order as expected in one dimension.

lowest energy state is maximally occupied, and F ordering is restored. The qualitative picture emerging from the effective spin model is able to reproduce the salient features of the RH model, both in terms of the phase boundary and in terms of the pattern of broken symmetry phases [44], at least for moderate values of g . At yet higher coupling g , even higher states become occupied sequentially when resonances between excited state energy levels occur. The occupation of these higher levels demonstrates the eventual failure of the effective spin 1/2 model at large g .

MPO results.—A natural question is whether our mean field analysis survives strong quantum fluctuations in low dimensions. In this respect, the effective spin model has the advantage of being amenable to an exact numerical treatment with an infinite matrix product operator approach, which we now turn to describe. In Fig. 4 we show infinite matrix product operator results for spin correlators evaluated for $g'/g = 0.25$, $J = 0.5$ as a function of g at various separations l between sites [panel (a)] and as a function of separation l at various values of g . These numerically exact results confirm the ordering seen in mean field, specifically the sequence of F-AF-F upon increasing g , but additionally show that in low dimensions, fluctuations destroy long-range order in driven-dissipative systems, as expected. Further results are presented in the Supplemental Material [44] supporting this statement.

In summary, we have presented the steady-state phase diagram of the nonequilibrium Rabi-Hubbard model, using various mean-field-based techniques and a matrix product operator approach that can capture effects beyond mean field. The phase diagram of the nonequilibrium model was found to be far richer than the equilibrium analogue, exhibiting ferroelectric, antiferroelectric, and incommensurate ordering. In addition, the phase diagram was found to also exhibit limit-cycle solutions. The matrix product operator results confirm qualitatively the pattern of the phases.

The research data supporting this publication can be accessed at <http://dx.doi.org/10.17630/a8829c09-7d49-4472-8e9e-f8219b53d640>.

H. E. T. acknowledges support through NSF Grant No. DMR-1151810 and The Eric and Wendy Schmidt Transformative Technology Fund. C. J. and J. M. J. K. acknowledge support from the EPSRC program “TOPNES” (EP/I031014/1). J. M. J. K. acknowledges support from the Leverhulme Trust (IAF-2014-025). R. F. acknowledges support from EU (IP-SIQS and QUIC). We are grateful to C. Aron for help in preparing Fig. 1. This work was supported in part by the National Science Foundation under Grant No. NSF PHY11-25915.

Mean-field calculations were performed by M. S., C. J., and M. B. MPO calculations were performed by C. J. R. F., J. K., and H. E. T. supervised the work.

-
- [1] J. Kasprzak, M. Richard, S. Kundermann, A. Baas, P. Jeambrun, J. M. J. Keeling, F. M. Marchetti, M. H. Szymańska, R. André, J. L. Staehli, V. Savona, P. B. Littlewood, B. Deveaud, and L. S. Dang, *Nature (London)* **443**, 409 (2006).
- [2] K. Baumann, C. Guerlin, F. Brennecke, and T. Esslinger, *Nature (London)* **464**, 1301 (2010).
- [3] J. Klaers, J. Schmitt, F. Vewinger, and M. Weitz, *Nature (London)* **468**, 545 (2010).
- [4] M. P. Baden, K. J. Arnold, A. L. Grimsmo, S. Parkins, and M. D. Barrett, *Phys. Rev. Lett.* **113**, 020408 (2014).
- [5] M. J. Bhaseen, J. Mayoh, B. D. Simons, and J. Keeling, *Phys. Rev. A* **85**, 013817 (2012).
- [6] J. Keeling, M. J. Bhaseen, and B. D. Simons, *Phys. Rev. Lett.* **105**, 043001 (2010).
- [7] I. Carusotto and C. Ciuti, *Rev. Mod. Phys.* **85**, 299 (2013).
- [8] D. E. Chang, V. Gritsev, G. Morigi, V. Vuletic, M. D. Lukin, and E. A. Demler, *Nat. Phys.* **4**, 884 (2008).
- [9] J. Otterbach, M. Moos, D. Muth, and M. Fleischhauer, *Phys. Rev. Lett.* **111**, 113001 (2013).
- [10] M. Hönig, D. Muth, D. Petrosyan, and M. Fleischhauer, *Phys. Rev. A* **87**, 023401 (2013).
- [11] F. Dalfó, S. Giorgini, L. P. Pitaevskii, and S. Stringari, *Rev. Mod. Phys.* **71**, 463 (1999).
- [12] B. M. Garraway, *Phil. Trans. R. Soc. A* **369**, 1137 (2011).
- [13] D. Nagy, G. Szirmai, and P. Domokos, *Phys. Rev. A* **84**, 043637 (2011).
- [14] B. Öztóp, M. Bordyuh, Ö. E. Müstecaplıoğlu, and H. E. Türeci, *New J. Phys.* **14**, 085011 (2012).
- [15] E. G. Dalla Torre, S. Diehl, M. D. Lukin, S. Sachdev, and P. Strack, *Phys. Rev. A* **87**, 023831 (2013).
- [16] M. Kulkarni, B. Öztóp, and H. E. Türeci, *Phys. Rev. Lett.* **111**, 220408 (2013).
- [17] F. Brennecke, R. Mottl, K. Baumann, R. Landig, T. Donner, and T. Esslinger, *Proc. Natl. Acad. Sci. U.S.A.* **110**, 11763 (2013).
- [18] L. M. Sieberer, S. D. Huber, E. Altman, and S. Diehl, *Phys. Rev. B* **89**, 134310 (2014).
- [19] L. M. Sieberer, M. Buchhold, and S. Diehl, [arXiv:1512.00637](https://arxiv.org/abs/1512.00637).
- [20] D. G. Angelakis, M. F. Santos, and S. Bose, *Phys. Rev. A* **76**, 031805 (2007).
- [21] M. J. Hartmann, F. G. S. L. Brandão, and M. B. Plenio, *Nat. Phys.* **2**, 849 (2006).
- [22] A. D. Greentree, C. Tahan, J. H. Cole, and L. C. L. Hollenberg, *Nat. Phys.* **2**, 856 (2006).
- [23] A. A. Houck, H. E. Türeci, and J. Koch, *Nat. Phys.* **8**, 292 (2012).
- [24] A. F. v. Loo, A. Fedorov, K. Lalumière, B. C. Sanders, A. Blais, and A. Wallraff, *Science* **342**, 1494 (2013).
- [25] M. Abbarchi, A. Amo, V. G. Sala, D. D. Solnyshkov, H. Flayac, L. Ferrier, I. Sagnes, E. Galopin, A. Lemaître, G. Malpuech, and J. Bloch, *Nat. Phys.* **9**, 275 (2013).
- [26] C. Eichler, Y. Salathe, J. Mlynek, S. Schmidt, and A. Wallraff, *Phys. Rev. Lett.* **113**, 110502 (2014).
- [27] T. Jacqmin, I. Carusotto, I. Sagnes, M. Abbarchi, D. D. Solnyshkov, G. Malpuech, E. Galopin, A. Lemaître, J. Bloch, and A. Amo, *Phys. Rev. Lett.* **112**, 116402 (2014).
- [28] J. Raftery, D. Sadri, S. Schmidt, H. E. Türeci, and A. A. Houck, *Phys. Rev. X* **4**, 031043 (2014).
- [29] J. A. Mlynek, A. A. Abdumalikov, C. Eichler, and A. Wallraff, *Nat. Commun.* **5**, 5186 (2014).
- [30] K. Le Hur, L. Henriot, A. Petrescu, K. Plekhanov, G. Roux, and M. Schiró, [arXiv:1505.00167](https://arxiv.org/abs/1505.00167).
- [31] F. Baboux, L. Ge, T. Jacqmin, M. Biondi, A. Lemaître, L. Le Gratiet, I. Sagnes, S. Schmidt, H. E. Türeci, A. Amo, and J. Bloch, *Phys. Rev. Lett.* **116**, 066402 (2016).
- [32] M. Schiró, M. Bordyuh, B. Öztóp, and H. E. Türeci, *Phys. Rev. Lett.* **109**, 053601 (2012).
- [33] M. Schiró, M. Bordyuh, B. Öztóp, and H. E. Türeci, *J. Phys. B* **46**, 224021 (2013).
- [34] T. Niemczyk, F. Deppe, H. Huebl, E. P. Menzel, F. Hocke, M. J. Schwarz, J. J. Garcia-Ripoll, D. Zueco, T. Hümmer, E. Solano, A. Marx, and R. Gross, *Nat. Phys.* **6**, 772 (2010).
- [35] G. Vidal, *Phys. Rev. Lett.* **91**, 147902 (2003).
- [36] G. Vidal, *Phys. Rev. Lett.* **93**, 040502 (2004).
- [37] M. Zwoleak and G. Vidal, *Phys. Rev. Lett.* **93**, 207205 (2004).
- [38] R. Orús and G. Vidal, *Phys. Rev. B* **78**, 155117 (2008).
- [39] Special issue, edited by F. Wilczek [U. Schollwöck, *Ann. Phys. (Amsterdam)* **326**, 96 (2011)].
- [40] F. Dimer, B. Estienne, A. S. Parkins, and H. J. Carmichael, *Phys. Rev. A* **75**, 013804 (2007).
- [41] D. Ballester, G. Romero, J. J. García-Ripoll, F. Deppe, and E. Solano, *Phys. Rev. X* **2**, 021007 (2012).
- [42] A. L. Grimsmo and S. Parkins, *Phys. Rev. A* **87**, 033814 (2013).
- [43] L. J. Zou, D. Marcos, S. Diehl, S. Putz, J. Schmiedmayer, J. Majer, and P. Rabl, *Phys. Rev. Lett.* **113**, 023603 (2014).
- [44] See Supplemental Material at <http://link.aps.org/supplemental/10.1103/PhysRevLett.116.143603> for further details of the Raman driving scheme, the effective model, and further MPO results.
- [45] L. P. Kadanoff, *Statistical Physics: Statics, Dynamics and Renormalization* (World Scientific, Singapore, 2000).
- [46] A. Le Boité, G. Orso, and C. Ciuti, *Phys. Rev. A* **90**, 063821 (2014).
- [47] T. E. Lee, H. Häffner, and M. C. Cross, *Phys. Rev. A* **84**, 031402 (2011).
- [48] J. Jin, D. Rossini, R. Fazio, M. Leib, and M. J. Hartmann, *Phys. Rev. Lett.* **110**, 163605 (2013).
- [49] M. Ludwig and F. Marquardt, *Phys. Rev. Lett.* **111**, 073603 (2013).
- [50] C.-K. Chan, T. E. Lee, and S. Gopalakrishnan, *Phys. Rev. A* **91**, 051601 (2015).
- [51] S. H. Strogatz, *Nonlinear Dynamics and Chaos* (Perseus Books, Cambridge, MA, 1994).
- [52] C. Joshi, F. Nissen, and J. Keeling, *Phys. Rev. A* **88**, 063835 (2013).